Muon Pair Production by 12-GeV/c Negative π and K Mesons on Carbon and Iron*

A. A. WEHMANN,† E. ENGELS, JR., C. M. HOFFMAN, P. G. INNOCENTI,‡ AND RICHARD WILSON
Harvard University, Cambridge, Massachusetts 02138

AND

W. A. BLANPIED
Case-Western Reserve University, Cleveland, Ohio 44106

AND

D. J. DRICKEY§
Stanford Linear Accelerator Center, Stanford University, Stanford, California 94305

AND

L. N. HAND
Cornell University, Ithaca, New York 14850

AND

D. G. STAIRS
McGill University, Montreal, Quebec, Canada

(Received 27 September 1968)

The apparatus, method of data analysis, and results of a spark-chamber experiment on the production of muon pairs by 12-GeV/c π^- and K^- mesons incident on carbon and iron are discussed in detail. Based on these measurements, the best values for the ρ^0-meson mass and width are $M_\rho = 765 \pm 7$ MeV and $\Gamma_\rho = 95 \pm 19$ MeV, while the branching ratio $\Gamma(\rho^0 \to \mu^+\mu^-)/\Gamma(\rho^0 \to \pi^+\pi^-) = (5.6 \pm 1.1) \times 10^{-5}$. Values of the spin-density matrix elements $\rho_{\lambda\lambda'}$ for the dimuon system in the mass range $600 \leq M_{\mu\mu} \leq 900$ MeV are given as functions of the square of the momentum transfer from the incident particle. Results of a qualitative study of the $\mu^-\mu^+\pi^-$ system are reported. A value for the branching ratio $\Gamma(\phi^0 \to \mu^+\mu^-)/\Gamma(\phi^0 \to \text{all})$ and upper limits on decay modes $\Gamma(\eta^0 \to \mu^+\mu^-)/\Gamma(\eta^0 \to \text{all})$ and $\Gamma(\eta^0 \to \pi^0\mu^+\mu^-)/\Gamma(\eta^0 \to \text{all})$ are also given. The invariant-mass spectrum of the muon pairs shows no evidence for the existence of a $J = 1^-$ isovector meson, other than the ρ^0, up to 1300 MeV.

I. INTRODUCTION

SEVERAL results of a spark-chamber experiment on the production of muon pairs by 12-GeV/c π^- and K^- mesons incident on carbon and iron have been reported previously.[1-3] References 1 and 2 give values of the spin-density matrix elements $\rho_{\lambda\lambda'}$ for the dimuon system in the mass range $600 \leq M_{\mu\mu} \leq 900$ MeV, and a value for the branching ratio

$$\Gamma(\rho^0 \to \mu^+\mu^-)/\Gamma(\rho^0 \to \pi^+\pi^-).$$

Reference 3 reports on a determination of the branching ratio

$$\Gamma(\phi^0 \to \mu^+\mu^-)/\Gamma(\phi^0 \to \text{all}),$$

and in addition gives upper limits on branching ratios for two rare muon-pair decay modes of the η^0 meson and a comparison of the present experimental results with those from μ-p scattering measurements.

This paper gives a more complete review of the experiment, summarizing the results already reported and giving several new ones. Section II describes the apparatus, while Sec. III contains a detailed account of the procedures used in data reduction and analysis, in particular, of the dimuon polarization analysis. Section IV describes the details of four methods used to determine the muon pair branching ratio of the ρ^0 meson. Results and conclusions appear in Sec. V. Section V A gives a determination of the ρ^0 mass and width, Sec. V B discusses the muon-decay angular distributions and gives the best fits to the density matrix elements $\rho_{\lambda\lambda'}$ in the dimuon mass region $600 \leq M_{\mu\mu} \leq 900$ MeV as a function of the momentum transfer between the incident particle and the dimuon system. The four determinations of the muon pair branching ratio of the ρ^0 meson are summarized in Sec. V C together with published values of the ρ^0 leptonic branching ratios reported by other investigators. Section V D gives the results of a qualitative study of the $\mu^+\mu^-\pi^-$ system, while Sec. V E recapitulates several of the conclusions from Refs. 2 and 3.

* Work supported by the U. S. Atomic Energy Commission and the Canadian National Research Council.

† Present address: Physics Department, University of Rochester, Rochester, N. Y.

‡ Present address: CERN, Geneva, Switzerland.

§ Present address: Physics Department, University of California, Los Angeles, Calif.

[1] A. A. Wehmann, E. Engels, Jr., L. N. Hand, C. M. Hoffman, P. G. Innocenti, Richard Wilson, W. A. Blanpied, D. J. Drickey, and D. G. Stairs, Phys. Rev. Letters **17**, 1113 (1966).

[2] A. A. Wehmann, E. Engels, Jr., C. M. Hoffman, P. G. Innocenti, Richard Wilson, W. A. Blanpied, D. J. Drickey, L. N. Hand, and D. G. Stairs, Phys. Rev. Letters **18**, 929 (1967).

[3] A. A. Wehmann, E. Engels, Jr., C. M. Hoffman, P. G. Innocenti, Richard Wilson, W. A. Blanpied, D. J. Drickey, L. N. Hand, and D. G. Stairs, Phys. Rev. Letters **20**, 748 (1968).

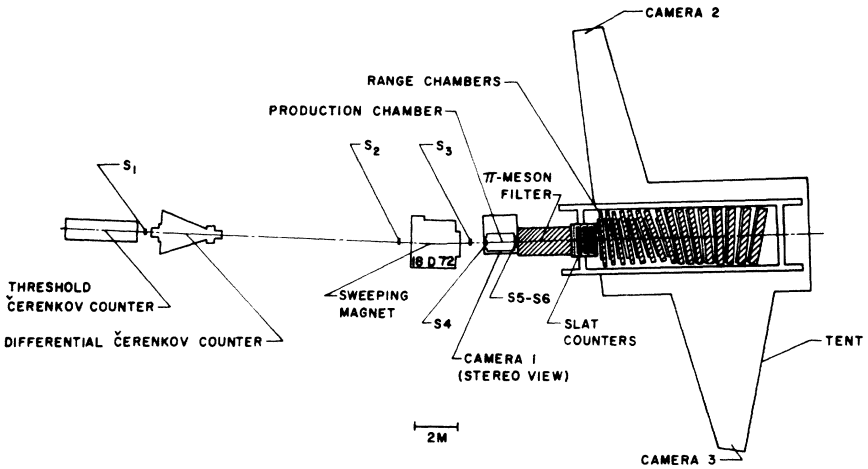

FIG. 1. Experimental apparatus. A 12-GeV/c negative secondary beam was incident upon the production spark chamber which contained forty-two $\frac{1}{2}$-in. plates, and served as the external target. Iron plates were used during about one-half the runs, carbon plates during the remaining runs. The threshold and differential Čerenkov counters in combination were used to tag K mesons and antiprotons, while the sweeping magnet deflected low-energy muons away from the chamber axis. The $6\frac{1}{2}$-ft iron π-meson filter behind the production chamber absorbed virtually all strongly interacting particles that were incident on the apparatus or produced in the chamber. Counters S_1, S_2, and S_3 were 3×3-in. scintillators, S_4 an 18-in. scintillator with a 3-in.-diam hole centered on the beam axis, S_5–S_6 a pair of 9×18-in. scintillators placed on either side of the beam axis. Each of the four slat banks consisted of 12 vertically oriented 4×48-in. scintillation counters arranged in square arrays and separated from the succeeding slat bank by a 6-in. thickness of lead. The system was triggered on a signal generated by $S_1S_2S_3\bar{S}_4$ in coincidence with at least two counters in each of the four slat banks. Muon energies were measured by photographing their stopping positions in a series of 17 aluminum range chambers interspersed between steel plates.

II. APPARATUS

The experimental apparatus was designed to detect muon pairs produced with a probability on the order of 10^{-6} relative to the expected dominant background:

$$\pi^- + \text{nucleus} \rightarrow \rho^0 + \text{anything}$$
$$\searrow$$
$$\pi^+ + \pi^-,$$

and to detect such dimuon states with invariant masses up to about 1300 MeV with good efficiency. A plan view is shown in Fig. 1. The secondary beam transport system, shown in Fig. 2, is described in detail elsewhere.[4] The beam was produced at 4.5° to the circulating proton beam on a beryllium wire target in the AGS G–10 straight section, and had a central momentum of 11.4 GeV/c during runs in which muon pairs were produced on iron, and 12.1 GeV/c during production runs on carbon. In both cases, its momentum spread (full width at half-maximum) was about 4%. The beam had an intensity on the order of 10^5/pulse, and consisted primarily of π^- mesons, with about 5% K^- mesons and 1% antiprotons. A threshold and a differential Čerenkov counter in combination (Fig. 1) identified the latter two particles. Whenever one of them produced an event which triggered the spark chambers, an appropriate data light was photographed along with the production chamber. However, fewer than 50 interesting K^--produced events (Ref. 3) and no interesting $\bar{p}$ events were detected. Observation of the latter class of events with reasonable efficiency would have required an apparatus capable of detecting muon pairs with invariant masses greater than twice the nucleon rest mass. The incident beam also contained a number of decay muons. Those with low energies were deflected into the anticoincidence counter, S_4, so that such muons could not directly trigger the spark chambers, although they did contribute to the background. The remaining high-momentum muons constituted 1–2% of the incident beam.

Muon pairs were produced in a production spark chamber consisting of forty-two $\frac{1}{2}$-in. plates. Iron plates were used during approximately one-half the runs, carbon plates during the remaining runs. Interactions in the production chamber were photographed in 90° stereo vision.

A 6.5-ft-long iron π-meson filter, placed immediately behind the production chamber, was designed to absorb most of the π mesons as well as any other strongly interacting particles produced in the chamber. This filter was followed by forty-eight, 4×48-in., vertically oriented trigger scintillation counters (hereafter referred to as slat counters) placed side by side in groups of 12 to form four 48×48-in. banks. Each counter bank was separated from the preceding one by 6 in. of lead. The requirement of the simultaneous traversal of charged particles through at least two of the slat counters in each of the four banks, together with the lead absorber between the banks, served to eliminate triggers due to knock-on electrons in coincidence with beam muons.

The energy of the muons that successfully traversed the π-meson filter and slat counter banks was determined by measuring their ranges in 3200 g/cm² of steel

[4] A. L. Read and R. Rubinstein, Brookhaven National Laboratory Report No. 9213 (unpublished).

that followed the counters. The steel, which consisted of vertically suspended plates of battleship armor, was interspersed between seventeen 2-gap aluminum spark chambers. The first ten of these range chambers had dimensions 6×6 ft and the remaining seven measured 8×8 ft. The thickness of the steel plates was increased in the downstream direction in order to maintain a constant percentage range uncertainty along the path of the stopping particles. Muons whose total energies in the production chamber were between about 4 and 10.5 GeV stopped in this range-measuring array, the lower limit being set by their energy loss in the iron and lead preceding it. The range chambers were photographed from the side as shown in Fig. 1. The energy calibration of the array is discussed in the Appendix.

The spark-chamber system was triggered by an incident beam particle in coincidence with a pair of counters in each of the four slat banks behind the π-meson filter. The coincidence $S_1S_2S_3\bar{S}_4$ defined the incident beam. Counters S_1, S_2, and S_3 were 3×3-in. scintillators, S_4 an 18×18-in. scintillation counter with a 3-in.-diam hole centered on the beam line. The addition of the anticoincidence signal from S_4 to the trigger logic reduced the number of triggers in which at least one of the two particles registering in the slat banks was a beam muon, since (as already noted) the final magnet in front of the production chamber deflected low-energy muons into S_4. During the runs with carbon plates in the production chamber the two 9×18-in. counters S_5S_6 placed symmetrically to the left and right of the beam line were added to the coincidence logic in order to set a bias against triggers resulting from single particles exiting from the production chamber.

The 6.5-ft iron filter behind the production chamber was designed primarily to absorb π mesons from the decay $\rho^0 \rightarrow \pi^+\pi^-$ before they decayed into muons which would have been capable of triggering the system. With carbon plates in the production chamber it was estimated that the combined probability of (i) two π mesons decaying into muons before being absorbed, (ii) two π mesons escaping absorption and directly simulated a muon pair in the slat counters, and (iii) one π meson decaying with the other escaping absorption was on the order of 10^{-6}, and thus contributed about a 2% background to the direct muon-pair events. When iron plates were used in the chamber these background estimates were reduced by about a factor of 2. In order to provide experimental confirmation of these estimates, a series of runs was made with the carbon plate spark chamber moved about 13 ft upstream from its normal position in order to increase the probability of π-meson decay in flight before the filter.

In addition to these three direct coherent background sources, there were related backgrounds in which a $\rho^0 \rightarrow \pi^+\pi^-$ decay appeared in the production chamber while two beam muons or a beam muon and a decay muon triggered the system. The magnitude of these backgrounds was estimated from the known fraction of

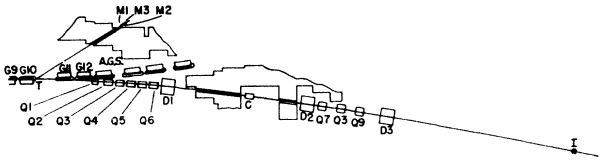

FIG. 2. Secondary beam transport system. (For details see Ref. 4.) The 12-GeV/c negative beam was produced on an internal beryllium wire target (T) located in AGS straight section G10 (upstream from AGS magnet G10) at 4.5° to the circulating proton beam, and was brought to a focus at I, the center of the production chamber. $Q1$ and $Q2$ were 32-in.-long 8-in.-aperture quadrupoles ($8Q32$), $Q3$-$Q9$ 48-in.-long 8-in.-aperture quadrupoles ($8Q48$), and $D1$-$D3$ 6-in.-gap 72-in.-long uniform-field bending magnets (18D72). A fourth 18D72 magnet located immediately in front of the focal point I (the sweeping magnet of Fig. 1) is not shown. The collimator (C) was 40 in. long, $\frac{1}{2}$ in. wide, and 1 in. high.

events in which both a high-energy beam muon (identified as such by its range) *and* a bona fide muon-pair decay appeared in the chambers. It was a more serious problem for the carbon than for the iron runs, since in the latter case one or both of the π mesons almost always scattered in the iron plates, and the event was therefore rejected by the scanning criteria (Sec. III).

III. DATA REDUCTION AND ANALYSIS

The production- and range-chamber photographs were first scanned to select and classify the events prior to measurement. All events with more than one incoming track in the production chamber were rejected unless the extra tracks terminated in the first half of the chamber. An interaction vertex in a fiducial volume between the 6th and 30th plate with at least two but no more than four straight charged-particle tracks emerging from it was required. Two of these tracks were required to exit from the chamber and to be correlated reasonably well with stopping tracks in the range chambers. The range-chamber module in which each track terminated was recorded at the time of scanning.

Events to be measured were classified into two groups:

(1) Two-prong events were defined as those in which two and only two tracks (other than the incident track) appeared in the production chamber. In view of the above cited scanning criteria both of these had to be attached to the interaction vertex, exit from the chamber, and be correlated with stopping tracks in the range modules. Any subsequent prongs attached to the outgoing tracks (δ rays, for instance) could be no more than two sparks long.

Since the iron-plate spark chamber contained about 25 radiation lengths of material, two-prong events in this chamber were mostly of the type

$$\pi^- + p \rightarrow \mu^+ + \mu^- + n.$$

A small fraction of the two-prong events in the carbon-plate chamber also contained a π^0 meson in the final state (see Sec. IV).

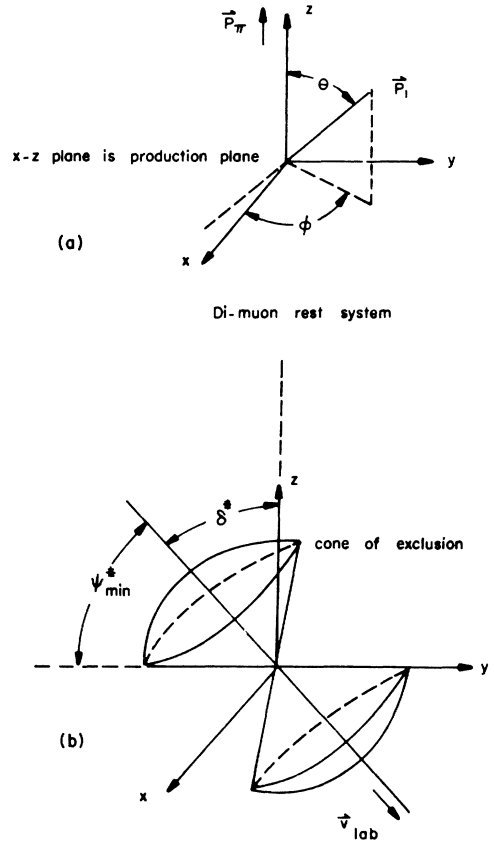

FIG. 3. (a) Definition of the muon decay angles θ and ϕ in the dimuon rest frame. (b) Origin of the most serious bias on the muon angular distributions. Any muon whose momentum vector $\mathbf{p}_1^*$ $(=-\mathbf{p}_2^*)$ in the dimuon rest frame fell within the cone of exclusion defined by the angles δ^* and $\psi_{\min}^*$ would have had insufficient laboratory energy to traverse the slat counter banks and trigger the spark-chamber system. The axis of the cone is defined by the angle δ^* which is related to δ, the dimuon production angle in the laboratory, by

$$\tan\delta^* = \sin\delta/\gamma(\cos\delta - \beta_0/\beta_\pi),$$

with β_0 the velocity of the dimuon system in the laboratory. The opening angle of the cone is given by

$$\cos\psi_{\min}^* = (1/\beta_0 p_1^*)(\tfrac{1}{2}M_{2\mu} - E_{\min}/\gamma_0),$$

where $M_{2\mu}$ is the invariant dimuon mass and $E_{\min}$ the minimum muon energy required to traverse the π-meson filter and the four slat counter banks.

(2) Multiprong events (which satisfied the scanning criteria) could have up to four charged tracks emerging from the interaction vertex, but two and only two exiting from the chamber. The two-spark subsequent prong requirement was retained. However, events with any number of tracks separated from the interaction vertex were acceptable. A subclass of three-prong events was subsequently selected from the multiprong events in carbon in an attempt to study the $\rho^0\pi^-$ final state (Sec. V D). These events were required to have a clean vertex (i.e., no short tracks in the vicinity), and three outgoing tracks, two of which exited from the chamber. The third track was allowed to interact after five plates provided the two muons in the range chamber could be associated with the other two production-chamber tracks by their positions and directions. In addition, the two range-chamber tracks were required to be tightly correlated with production-chamber tracks.

At a later stage in the analysis the scanning criteria were relaxed in order to improve the statistics on those events for which the identification lights on the production chamber indicated that the incident particle was a K^- meson. In these cases, any number of incoming tracks were allowed in the chambers, and any number could emerge from the vertex provided at least two and no more than three exited from the chamber and were reasonably straight. Subsequent prongs were also permitted if the outgoing track to which they were attached did not alter its direction as a consequence.

Track measurements were made using film-plane digitizers. Five points were normally measured on the incident track and on each outgoing track in each of the two 90° stereo-vision production-chamber views. Reconstruction of the measured points in the three-dimensional space of the production chamber was carried out using a standard type of computer program. Linear fits to each track were then attempted. Each point was weighted with a constant measuring error and with a factor that varied with the $\frac{3}{2}$ power of its distance from the vertex and inversely with the momentum of the corresponding particle as determined from the range data. The latter weight function was intended to allow for expected increases in the deviation of the track from linearity due to multiple scattering in the chamber plates.

In examining fits to the first sets of measured data a significant break was found between those with χ^2 corresponding to less than 2.5 and those with χ^2 corresponding to more than 4.5 standard deviations. When observed visually, tracks in the latter category usually exhibited considerable curvature or had an obvious kink. Hence a χ^2 corresponding to 3 standard deviations was chosen as the criterion for a good fit. If a fit to a given track failed to meet this criterion, the point giving the greatest contribution to the large χ^2 was dropped and another fit attempted with the remaining points alone. If the refitted line also failed to meet the acceptability criterion, a fit was attempted to a form having a term that varied as the $\frac{3}{2}$ power of the distance from the vertex in an attempt to introduce some curvature due to multiple scattering. If this fit also failed, the entire event was rejected. Of 385 events in iron that satisfied the two-prong scanning criteria, only 22 were rejected because of bad fits. A similar rejection ratio was found for two-prong events in carbon.

Slopes at the vertex were calculated relative to the production-chamber coordinates in two perpendicular planes containing the nominal beam direction for all measured tracks satisfying the fitting criteria. Given these slopes, together with the incident beam energy (corrected, in the case of iron, for ionization losses in

the spark-chamber plates), and the outgoing muon energies from the range chambers, all necessary kinematic quantities could be calculated. In particular, $M_{\mu\mu}$, the invariant dimuon mass, $-t$, the square of the four-momentum transfer to the muon pair, as well as the decay angles in the dimuon rest frame were determined.

Errors in the measured dimuon masses and four-momentum transfers were due to uncertainties in the muon energies and the measured track angles. As previously noted, the latter uncertainty is due both to measurement error and multiple scattering in the production-chamber plates. The rms error in $\Delta M_{\mu\mu}/M_{\mu\mu}$ was 8.4% in the iron-plate chamber and 5.3% for the carbon chamber for symmetric energy events in the region of the ρ^0 peak. The errors were somewhat larger for highly asymmetric events. The error in $-t$ for an event symmetric in both the angle and the energy of the two muons was about 0.023 $(\mathrm{GeV}/c)^2$, and increased somewhat away from symmetry.

The output data from the reconstruction program was corrected for two broad categories of inefficiencies: (1) those inherent in the geometry of the experimental apparatus, and (2) those that entered during the scanning and measuring operations. The latter category included legitimate events that were not measured because of a misapplication of the scanning criteria; events rejected because of excessive complications such as straight-through beam tracks in the production chamber, subsequent tracks on the outgoing prongs more than two sparks long, or more than four prongs emerging from the vertex; and legitimate events with one or more prongs that did not pass the fitting criteria. Corrections for the first two types of loss were estimated by rescanning events taken from several different rolls of production chamber film. In order to correct for the third type of loss, it was assumed that the distributions of such events in both invariant mass and momentum transfer were the same as the distributions for the accepted events.

There were three sources of geometric inefficiencies: (a) the minimum energy requirement on the decay muon, (b) the requirement that the two members of each muon pair had to pass through two different counters in each of four slat banks, and (c) the angular limits imposed by the range chambers.

The origin of the type (a) inefficiency [hereafter called kinematic to contrast it with types (b) and (c)] is best understood by referring to Fig. 3(a) which defines the muon-decay angles, θ and ϕ, in the dimuon rest frame. This frame is oriented so that the incident π meson is along the z direction and the dimuon system is produced in the xz plane. Figure 3(b) shows an excluded cone in the dimuon rest system defined by the angles δ^*, which depends upon the production angle of the dimuon system in the laboratory, and $\psi_{\min}{}^*$. The latter is the minimum decay angle for a muon with a given center-of-mass energy such that its laboratory energy is greater than the minimum-energy muon that can pass through the π-meson filter and be detected in the slat counters (3.93 GeV for iron, 3.71 GeV for carbon). If the muon's center-of-mass angle fell within the excluded cone the event would not have triggered the system. Thus the lower-energy cutoff leads to a bias in the measured angular distributions. Since the angle $\psi_{\min}{}^*$ is a function of the velocity of the dimuon rest system as well as energy of the muons in this system, it differed for each event and was calculated, along with δ^*, as one of the kinematic variables in the reconstruction program.

The treatment of this kinematic bias was complicated by its dependence on the form of the bias-free production angular distributions whose determination was a primary goal of the experiment. Therefore, it was necessary to incorporate the biases explicitly into a maximum-likelihood fit that was made to determine the best values of the spin-density matrix elements $\rho_{\lambda\lambda'}$ of the decaying dimuon system. The best fits to $\rho_{\lambda\lambda'}$ in turn gave an average efficiency for each event, and these were used to determine sets of weighted-mass histograms and angular distributions.

If the decaying dimuon system is a $J=1^-$ meson produced in a π^--nucleon interaction by means of a peripheral mechanism, it can be shown[5] that the distribution of the muon angles θ and ϕ in the dimuon rest system is

$$W(\theta,\phi)=\frac{1-\frac{4}{3}\pi\beta^2 W'(\theta,\phi)}{4\pi(1-\frac{1}{3}\beta^2)},$$

where β is the velocity of either muon in this system. $W'(\theta,\phi)$, the corresponding angular distribution for the decay $\rho^0\to 2\pi$, is[6]

$$W'(\theta,\phi)=(\tfrac{3}{4}\pi)[\rho_{0,0}\cos^2\theta+\rho_{1,1}\sin^2\theta-\rho_{1,-1}\sin^2\theta\cos 2\phi-\sqrt{2}\mathrm{Re}\rho_{1,0}\sin 2\theta\cos\phi].$$

The $\rho_{\lambda\lambda'}$ are the above-cited spin-density matrix elements for the decaying vector meson. From the general properties of the spin-density matrix and from parity conservation in the production reaction, it can be shown that[6]

$$2\rho_{1,1}+\rho_{0,0}=1,$$
$$|\rho_{1,-1}|\leq\rho_{1,1},$$
$$\mathrm{Re}\rho_{1,0}\leq(\rho_{0,0}\rho_{1,1})^{1/2}.$$

For production of a $J=1^-$ meson by an unmodified scalar-exchange mechanism, $\rho_{0,0}=1$ and all other elements are zero, while production via an unmodified vector exchange gives $\rho_{0,0}=0$. The form of $W(\theta,\phi)$ is not altered if absorption effects are introduced into the production mechanism, but the predicted values of the matrix elements are.

[5] R. J. Oakes, Nuovo Cimento 44A, 440 (1966).
[6] K. Gottfried and J. D. Jackson, Nuovo Cimento 34, 735 (1964).

The philosophy of the maximum-likelihood method stresses the use of a *normalized* distribution, since the likelihood function itself may be regarded as an inverse probability function.[7] In the present instance, the distribution in $W(\theta,\phi)$ should be normalized to a 4π solid angle. However, because of the lower-energy cutoff of the apparatus, a given detected event defined by a particular set of the angular variables θ_i, ϕ_i, δ_i^*, ψ_i^* did not have inverse probability $W(\theta_i,\phi)$. Rather it had likelihood

$$W(\theta_i,\phi_i)/\eta_a,$$

where

$$\eta_a \equiv \int_{\Delta\Omega_i} W(\theta,\phi)d\Omega.$$

Here $\Delta\Omega_i$ is that portion of the unit sphere which is not excluded in Fig. 3(b) and evidently depends on δ_i^* and $\psi_{\min}^*$. If η_b and η_c, the second and third inefficiencies cited above, are included then the likelihood for the ith event becomes

$$W(\theta_i,\phi_i)/\epsilon_i,$$

where $\epsilon \equiv \eta_a\eta_b\eta_c$ is the inverse weight of the ith event. All three efficiencies are functions of the kinematic variables of the event, and η_a depends on the values of the density matrix elements ρ_{ij} as well.

The second source of geometric inefficiency arose from the fact that the two members of a muon pair were each required to traverse a different counter in each of the four slat banks. Thus, an event with a roughly vertical decay plane would not have triggered the system. To determine the corresponding efficiency factor η_b for each acceptable event, the computer program rotated the outgoing pair about the incoming beam axis in order to simulate a population of 100 events distributed azimuthally about the beam. This population of pseudo-events was then examined to determine η_b, the fraction in which both outgoing tracks fell into different slat counters.

The same calculation was used to determine the third geometric efficiency factor of each event, η_c. The absolute upper limit of a muon angle relative to the production-chamber coordinates was determined by the size of the tenth range-chamber module which was the last 6×6-ft module, and depended on both the energy of the muons and their laboratory decay angles. For a pair with $E_1=E_2=5.5$ GeV produced with equal angles relative to the nominal beam axis, this restriction implied an upper limit of 1270 MeV on the dimuon mass. Since the range modules were square the angular limit was a function of the azimuthal orientation of the dimuon decay plane. The fraction of the azimuthal population so excluded was by definition $(1-\eta_c)$. Any event one of whose tracks was observed in the ninth module but which would have missed the tenth module because of its angular divergence was excluded from the sample. Very few fell into this category.

After the efficiencies η_b and η_c for each of the N events in a given class (i.e., iron two-prong, iron multiprong, carbon two-prong, and carbon multiprong) had been calculated, the product

$$\mathfrak{L} = \prod_{i=1}^{N} \frac{W_i(\theta_i,\phi_i)}{\epsilon_i}$$

was formed using a trial set of matrix elements $\rho_{\lambda\lambda'}$ in $W_i(\theta_i,\phi_i)$ and η_a. The $\rho_{\lambda\lambda'}$ were then varied until $\mathfrak{L}$ was maximized, and the resulting ϵ_i for each event defined as its inverse weight. Events with $\epsilon_i<0.02$ were excluded from the sample while those with $0.02\leq\epsilon_i\leq 0.1$ were assigned $\epsilon_i=0.1$. The average value of ϵ_i for events in the vicinity of the ρ^0 peak and with $-t<0.3$ $(\mathrm{GeV}/c)^2$ was about 0.3, and as expected decreased with both variables to an average value of 0.2 at $M_{\mu\mu}=1000$ MeV, $-t\sim 0.6$ $(\mathrm{GeV}/c)^2$. Uncertainties in the best values for the density matrix elements were assumed to be statistical, and were determined from the maximized likelihood function. Values for $\rho_{\lambda\lambda'}$ are given in Table I and Fig. 6 (Sec. V B).

IV. CALCULATION OF $\varrho^0 \to 2\mu$ BRANCHING RATIO

A primary goal of the experiment was to obtain a value of the branching ratio

$$R=\Gamma(\rho^0\to\mu^+\mu^-)/\Gamma(\rho^0\to\pi^+\pi^-),$$

which would be equal to the measured cross-section ratio

$$\sigma_T(\rho^0\to\mu^+\mu^-)/\sigma_T(\rho^0\to\pi^+\pi^-),$$

if the ρ^0 mesons were produced in the same manner and the two decay modes measured with the same apparatus. Since these ideal circumstances were not applicable to the present experiment it was necessary to normalize data on ρ^0 production and decay via the dominant two-π-meson mode to our muon-pair rates. This was done in four different ways to obtain four different though not statistically independent determinations of the branching ratio. Results are summarized in Ref. 2 and in Table II of this paper (Sec. V C). We give here a detailed discussion of the procedure followed in arriving at these results, in addition to a slightly revised set of values for the results themselves.

The ρ^0-production cross-section data required in the denominator of the above branching-ratio expression were obtained from a number of bubble-chamber experiments. One set of these data gave cross sections for production by π^- mesons incident on liquid hydrogen

[7] J. Orear, University of California Radiation Laboratory Report No. UCRL 8417, 1958 (unpublished).

with a single-neutron recoil.[8] A second set provided production cross sections on a heavy liquid (C_2H_5Cl), and included both single-neutron-recoil events and events with more complicated final states.[9]

The nature of the production determined the class of muon-pair events used in calculating the cross section appearing in the numerator of the cross-section ratio for each of the four branching-ratio determinations. Muon data from two-pronged events in (1) iron and (2) carbon which consisted primarily of events with single-neutron recoils in the final states were paired with the liquid-hydrogen bubble-chamber data. These two muon-pair cross sections were calculated on the basis of invariant-mass spectra weighted in accord with the procedure outlined in Sec. III. The heavy-liquid bubble-chamber cross section for single-neutron-recoil events was paired with (3) muon-pair events in carbon with an analogous restriction imposed on the final state. Finally (4) a cross section determined from all muon-pair events in carbon with no more than four visible tracks in the final states was matched to the production cross section for the heavy-liquid bubble-chamber events on which the same restriction was imposed. In making the latter two determinations it was *not* necessary to use the weighted muon-pair histograms since, as explained below, it was possible to impose virtually the same experimental biases on the production data.

In calculating the muon-pair cross sections for two-prong events a number of corrections were applied to the data. The production spark chamber was not uniformly efficient in either angle or energy for detection of charged π mesons or γ rays from π^0 decay. Thus it was necessary to subtract an estimated number of events from the two-prong classes to correct for contamination by undetected π^- or π^0 mesons present in the final state. Estimates were $(18\pm12)\%$ for π^- contamination in both carbon and iron two-prong events, and $(10\pm6)\%$ for π^0's in iron and $(25\pm15)\%$ for π^0's in carbon.

No corrections were made for processes in which a neutron could appear in the spark chamber either by imparting some of its energy to a small number of protons in the nucleus in which interaction occurred, by charge-exchanging with a proton in the target nucleus, by picking up a π^+ from a proton, or by behaving in a similar fashion in a nucleus other than the target nucleus. The product of the total probability for these processes and the detection efficiency for the resulting charged particles in the spark chamber was sufficiently small to justify neglecting them.

Events with dimuon mass between 600 and 900 MeV were selected in order to isolate the ρ^0 peak appearing between these limits in the mass histograms. The experimental mass resolution of 127 MeV in iron and 94 MeV in carbon (full width at half-maximum) did not permit the separation of events in these peaks due to ρ^0 and ω^0 mesons, nor was it sufficiently good to show any ρ-ω interference effects. Selection of events with $|t|<0.3$ reduced the number of ω^0 events relative to the number of ρ^0 events, since the former are expected to be produced with a flatter momentum transfer distribution.[10] In order to determine the remaining fraction of ω^0 events in this low-momentum-transfer sample, known production cross sections for ω^0 and ρ^0 mesons in hydrogen with a single-neutron recoil[10] and an $SU(3)$ estimate[11] of the ratio of the two lepton-pair decay widths were used, leading to an estimate of 11%. An upper limit on the number of events due to the interference of the $\rho^0\to 2\mu$ and $\omega^0\to 2\mu$ amplitudes was established by assuming that production occurred in states with the same σ_z. This represented an upper limit because in reality, only absorption in the single-π-exchange diagram for ρ^0 production and in the π^0-exchange diagram for ω^0 production would permit them to populate the same J_z states.[12,13] In order to provide for possible interference effects in the data, the error on the estimate of the number of $\omega^0\to 2\mu$ events was increased so that, finally, it was assumed that $(11\pm11)\%$ of the low-t two-prong sample was not attributable to the process $\rho^0\to 2\mu$. No subtraction of background events in the region $600\leq M_{\mu\mu}\leq 900$ MeV was made. However, background estimates are reflected in the quoted uncertainties on the branching ratios.

In reducing the corrected muon-pair-event rates to cross sections per nucleus it was necessary to apply a thick-target correction due to the attenuation of the incident π^- mesons in the production-chamber plates. Several determinations of the π-meson attenuation length in iron and beryllium have been reported.[14] In addition, crude numbers for both carbon and iron were obtained from the distribution of vertices in the plates of the production chambers in the present experiment.

[8] The 150 ± 30-μb cross section for the reaction $\pi^-p\to\rho^0n$ was obtained from J. D. Jackson and J. T. Donahue (private communication), who based their estimate on an interpretation of the data from several liquid-hydrogen bubble-chamber experiments in the momentum range 1–8 GeV/c using the observed $1/p_\pi^2$ momentum dependence for the reaction.

[9] The heavy-liquid events were obtained in an exposure at CERN with 16-GeV/c π^- mesons using the Ecole Polytechnique heavy-liquid chamber described in M. Bloch, A. Lagarrigue, P. Rancon, and A. Rousset, Rev. Sci. Instr. **32**, 1302 (1961). We are grateful for the cooperation of Dr. H. H. Bingham in providing us with a magnetic tape containing these events, and for his extensive aid in our analysis of the data.

[10] E. Shibata and M. Wahlig, Phys. Letters **22**, 354 (1966).

[11] R. J. Rivers, Phys. Rev. **152**, 1263 (1966).

[12] J. D. Jackson, Rev. Mod. Phys. **37**, 484 (1965); J. D. Jackson, in *Proceedings of the Thirteenth Annual International Conference on High-Energy Physics, Berkeley, 1966* (University of California Press, Berkeley, 1967), p. 149.

[13] Interference between ω^0 and ρ^0 mesons decaying into lepton pairs, as observed in photoproduction experiments, can lead to as much as a 50% error in the $\rho^0\to 2\mu$ branching ratio [see R. G. Parsons and R. Weinstein, Phys. Rev. Letters **20**, 1314 (1968)]. This results from the production of both ρ^0 and ω^0 mesons via the same process—a diffraction mechanism. In contrast, different processes are involved in their production by π mesons.

[14] H. von Brieson, Jr., thesis, University of Rochester (unpublished); J. Tinlot, Brookhaven National Laboratory Report No. 750 (unpublished); J. Cox, F. Martin, M. L. Perl, T. H. Tan, T. F. Zipf, and W. L. Lakin, Stanford Linear Accelerator Center Report No. 434, 1968 (unpublished).

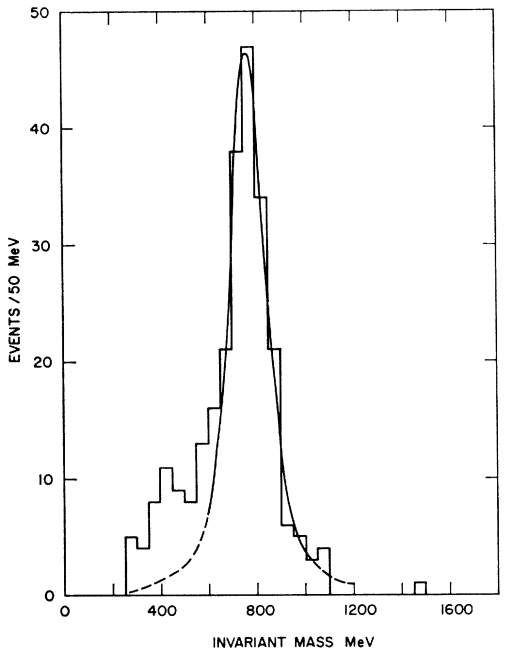

FIG. 4. The dimuon mass spectrum for two-pronged events produced on iron with $|t| \leq 0.3$ (GeV/c)^2. The histogram contains 177 events in the mass interval $600 \leq M_{\mu\mu} \leq 900$ MeV. A Breit-Wigner resonance curve, fitted to the data in this mass interval by means of a least-squares procedure, is superimposed.

A compromise value for iron obtained from all these sources was taken as 9.0±0.7 in. This was then scaled to carbon to give 24.0±1.5 in., in agreement with the mean free path obtained by scaling the beryllium data of Cox *et al.*[14]

Finally, before comparing the observed two-prong muon-pair data to the single-neutron-recoil ρ^0-production cross sections in liquid hydrogen, the former iron and carbon cross sections were scaled to free-proton cross sections. This was accomplished by means of an optical-model calculation which corrected for absorption of the incident π^- and outgoing ρ^0 mesons by the target nucleus. The resulting scale factors, which were used to convert from cross sections per nucleus to cross sections per free proton, were found to be 3.1±0.4 for iron and 2.0±0.25 for carbon. The slight differences between these values and those given in Ref. 2 are due to refinements made in the calculations subsequent to publication of that letter.

The heavy-liquid bubble-chamber cross sections used in the third and fourth determinations of the $\rho^0 \rightarrow 2\mu$ branching ratio were obtained from a selection of events from an exposure of the Ecole Polytechnique heavy-liquid bubble chamber in a 16-GeV/c π^- beam at CERN.[9] These events occurred in light nuclei and thus were closely analogous to the carbon events obtained in the present experiment. Hence, the error in scaling with atomic mass A was much smaller than in the case of comparison with hydrogen data, and it was possible to make use of all arbon events rather than just the two-prong events. In addition, the γ-ray conversion efficiency in this bubble chamber was much higher than in a hydrogen chamber. In principle this would have permitted an investigation of the number of π^0's contaminating the two-prong muon data but in practice this was nearly impossible.

Since a magnetic tape full of these heavy-liquid bubble-chamber events was available, it was possible to apply restrictions in energy and angle to the $\pi^+\pi^-$ combinations in final states with invariant dipion mass between 600 and 900 MeV. These restrictions simulated the trigger conditions on the final-state muons in our experiment, and practically eliminated the necessity for evaluating experimental inefficiencies due to these restrictions. It was only necessary to introduce a factor compensating for the differences in the decay distributions of the muons and π mesons. The detection efficiency due to these restrictions was estimated to be $\frac{2}{3}$ as large for $\rho^0 \rightarrow \pi^+\pi^-$ as for $\rho^0 \rightarrow \mu^+\mu^-$.

The heavy-liquid bubble-chamber events were classified into 24 categories. However, only the following categories with at least one $\pi^+\pi^-$ combination were of interest: $\pi^+\pi^-$, $\pi^+2\pi^-$, $\pi^+\pi^-\pi^0$, $\pi^+2\pi^-\pi^0$, $2\pi^+2\pi^-$, $2\pi^+3\pi^-$, $\pi^+2\pi^-2\mu$, $\pi^+\pi^-2\pi^0$, $\pi^+2\pi^-2\pi^0$, and $2\pi^+2\pi^-\pi^0$. Since only events in the first five categories had more than a negligible chance of surviving the simulated triggering restrictions, the remaining classes were subsequently neglected. Events in the former categories were reclassified according to whether (a) there was no proton track visible in the final state, (b) there was 1 proton visible in the final state, or (c) there was 1 backward or 2 forward proton tracks in the final state. The events used in the branching-ratio calculations included all three types of nucleon-recoil classification. However, the proton track was not included in the kinematic fitting since its kinematic variables were significantly altered inside the nucleus after the interaction. The total cross section per molecule for all events, along with the failure percentage of the kinematic fitting program and the scanning efficiency for each category, were all supplied along with the event tape[9]. Each of these cross sections was then cast into a form useful for comparison with our experimental results. This involved subtraction of backgrounds under the ρ^0 peaks, scaling from the 16-GeV/c π^- cross sections to 12 GeV/c and scaling from cross sections per molecule to cross sections per carbon atom. Two cross sections were obtained from the heavy-liquid bubble-chamber data for use in the denominator of the ρ^0 branching-ratio expression, namely, the cross section for the final state $\pi^+\pi^-$, and cross section for the sum of the five final states $\pi^+\pi^-$, $\pi^+2\pi^-$, $\pi^+\pi^-\pi^0$, $\pi^+2\pi^-\pi^0$, and $2\pi^+2\pi^-$. The former of these was compared directly with the muon-pair cross section extracted from our two-prong carbon data. The latter was used with the dimuon cross section derived from all the carbon data. No momentum-transfer restriction was imposed on the heavy-liquid data even

though only muon events with $|t| \leq 0.3$ (GeV/c)^2 were used in calculating the two-prong cross section. The error due to this discrepancy in momentum transfer is believed to be small. It was not possible to estimate the ω^0 contamination as accurately for the cross section based on all the carbon data as it was for the two-prong cross sections, simply because the available ω^0-production cross-section data are on hydrogen and are based on single-neutron-recoil events. Final states involving particles other than a single neutron were certainly present in the all-prong carbon data. Nevertheless, for lack of a better number, the ω^0 contamination was taken as $(11\pm11)\%$, as with the two-prong data. This figure is compatible with the estimated ratio of ω^0 to ρ^0 events in the heavy-liquid bubble-chamber data.[9]

V. RESULTS AND CONCLUSIONS

A. ρ Mass and Width

Figure 4 shows the measured dimuon mass spectrum for two-pronged events produced by the negative 12-GeV/c beam on iron, and subject to the restriction $|t| \leq 0.3$ (GeV/c)^2. The histograms contains 177 events in the mass interval $600 \leq M_{\mu\mu} \leq 900$ MeV. A Breit-Wigner resonance curve, shown superimposed on the histogram, was fitted to the data using a least-squares procedure. This fit was carried out without background subtraction. The dimuon mass resolution arising from the straggling of the muons in the iron interposed between the rear spark chambers and from errors in measuring the dimuon opening angle in the production chamber was 127 MeV (FWHM). After folding out the experimental resolution we obtain, from these iron data, $M_\rho = 765\pm7$ MeV, and $\Gamma_\rho = 95\pm19$ MeV. The errors arise from statistics and the uncertainty in our knowledge of the experimental resolution. A similar resonance curve was fit to the dimuon mass spectrum for two-pronged events produced on carbon, and yielded a width, subsequent to unfolding the experimental resolution, of 165 MeV. The large discrepancy between the widths obtained from the two classes of events is attributable to a considerably greater background in the case of carbon which would have been difficult to subtract without distorting the shape of the spectrum. There were three principal types of two-pronged background events: (1) $\rho^0 \rightarrow 2\pi$ events with both π mesons appearing in the production chamber while two beam muons which did not pass through the production chamber triggered the apparatus and appeared in the range chambers, (2) $\rho^0 \rightarrow 2\pi$ events in which one of the subsequent decay muons and a beam muon which did not pass through the production chamber triggered the apparatus and appeared in the rear chamber, and (3) $\rho^0 \rightarrow 2\pi$ events in which both subsequent decay muons triggered the apparatus. Contributions from the first and second sources were estimated from the number of two-pronged pictures in which one or more additional beam particles appeared in the production chamber, and were found to constitute from 10 to 20% of the total. Contributions from the second and third sources were estimated by comparing the dimuon mass histogram for low-momentum-transfer $[|t| \leq 0.3$ (GeV/c)$^2]$ two-pronged events obtained with the production chamber as close to the π-meson filter as possible, to the histogram obtained with the chamber moved 155 in. upstream from the filter to enhance the background from $\pi \rightarrow \mu$ decay events (Sec. II). In this way events from these two sources were found to constitute between 10–20% and on the order of 1%, respectively, of the total for the production chamber in its normal position near the π-meson filter. Since it seemed likely that an appreciable fraction of the two-pronged events on carbon were not $\rho^0 \rightarrow 2\mu$ events, the carbon data were rejected as a source of information on the ρ^0 mass and width, though not for the purpose of determining the $\rho^0 \rightarrow 2\mu$ branching ratio.

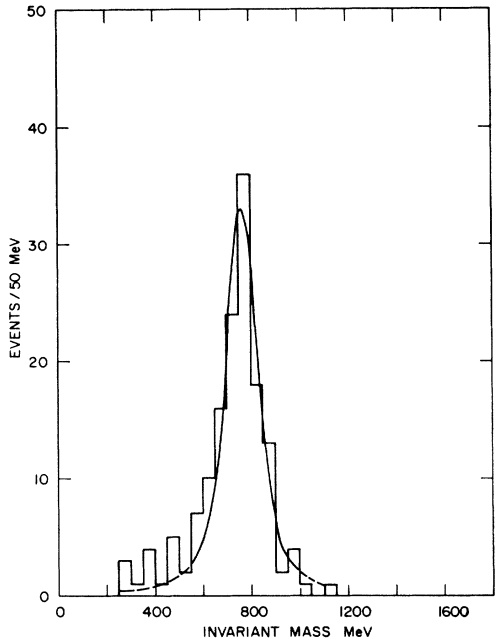

FIG. 5. The dimuon mass spectrum for three-pronged events produced on carbon with no momentum-transfer restriction. The histogram contains 107 events in the mass interval $600 \leq M_{\mu\mu} \leq 900$ MeV. A Breit-Wigner resonance curve, fitted to the data in this mass interval by means of a least-squares procedure, is superimposed.

The three types of background events mentioned in the last paragraph all involve the decay $\rho^0 \rightarrow 2\pi$. There was a negligible probability that at least one of these two π mesons would *not* have interacted in the iron-plate chamber and thus that one of these background events would have been counted as a $\rho^0 \rightarrow 2\mu$ event. Hence the assumption of a much larger coherent background in carbon than in iron seems reasonable, and we conclude that the quoted value $\Gamma_\rho = 95\pm19$ MeV represents the intrinsic width of the ρ^0 meson in our experiment.

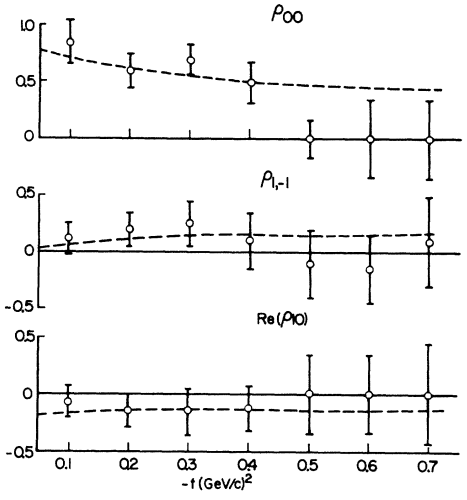

FIG. 6. Density matrix elements $\rho_{\lambda\lambda'}$ for the angular distributions of the decay muons as a function of momentum transfer to the dimuon system evaluated in the Jackson frame (Ref. 12). Two-pronged events on both carbon and iron were included in determining these parameters. The dashed curves give the results of a calculation based on production of the dimuon via one-pion exchange with absorption (Ref. 15).

The above interpretation of the background events in the carbon two-prong data is strengthened by evidence from an analysis of events in carbon in which three prongs emerged from the production vertex, and at least two of them exited from the rear of the production chamber. In order to determine which two of the three tracks were muons (the third was assumed to be a π meson), the two range-chamber tracks were extrapolated back to the production chamber on the scanning tables. Events for which such an extrapolation failed were rejected (Sec. III). Thus background events in which one or more beam muons triggered the system were not included in this sample. A Breit-Wigner resonance curve was fit to the dimuon mass spectrum from these three-pronged events (Fig. 5). After folding out the experimental resolution function from this resonance curve we obtain

$$M_\rho = 760 \pm 9 \text{ MeV}, \quad \Gamma_\rho = 100 \pm 23 \text{ MeV},$$

in agreement with the values determined from the iron two-prong data.

B. Decay Angular Distributions

Angular distributions of the decay muons in the dimuon rest system for two-pronged events in carbon with $600 \leq M_{\mu\mu} \leq 900$ MeV were presented in Ref. 2 both for $|t| \leq 0.3$ (GeV/c)^2 and for $|t| > 0.3$ (GeV/c)^2. The character of these distributions differ markedly in the two momentum-transfer regions. Angular distributions for two-pronged events on iron and multipronged events on carbon exhibit the same qualitative features.

As described in detail in Sec. III, these decay angular distributions can be parameterized in terms of a set of density matrix elements $\rho_{\lambda\lambda'}$ which are functions of t. Fig. 6 shows the values of these parameters obtained from a set of maximum-likelihood fits to events with $600 \leq M_{\mu\mu} \leq 900$ MeV and in momentum-transfer intervals 0.1 (GeV/c)^2 wide. In order to improve the statistics, iron and carbon two-pronged events were combined. The dashed curves shown in the figures give predictions for production of the dimuon system via a one-pion exchange with absorption.[15] The agreement with the theory below $|t| = 0.3$ (GeV/c)^2 suggests the dominance of the one-pion-exchange mechanism in this region.

TABLE I. Density matrix elements[a] for $600 \leq M_{\mu\mu} \leq 900$ MeV.

Event class	$\rho_{0,0}$	Re($\rho_{1,0}$)	$\rho_{1,-1}$
2-prong Fe, $\|t\| \leq 0.3$ (GeV/c)^2	0.70±0.10	0.10±0.10	0.15±0.15
2-prong Fe, $\|t\| > 0.3$ (GeV/c)^2	0.10±0.20	0.06±0.20	−0.05±0.2
2-prong C, $\|t\| \leq 0.3$ (GeV/c)^2	0.60±0.14	0.07±0.10	0.20±0.12
2-prong C, $\|t\| > 0.3$ (GeV/c)^2	0.10±0.13	0.02±0.20	−0.41±0.20
Multiprong C, $\|t\| \leq 0.3$ (GeV/c)^2	0.60±0.13	0.07±0.09	−0.02±0.12
Multiprong C, $\|t\| > 0.3$ (GeV/c)^2	0.10±0.13	0.00±0.16	−0.18±0.17

[a] Evaluated in the Jackson frame, Ref. 12. (See Fig. 3.)

Table I lists the values of the density matrix elements separately for iron two-pronged, carbon two-pronged, and carbon multipronged events in the range $600 \leq M_{\mu\mu} \leq 900$ MeV, both for $|t| < 0.3$ (GeV/c)^2 and $|t| > 0.3$ (GeV/c)^2.

C. $\varrho^0 \to 2\mu$ Branching Ratio

Muon-pair and ρ^0-production cross sections, determined by the procedures outlined in Sec. IV, are given in Table II along with the $\rho^0 \to \mu^+\mu^-$ branching ratio calculated in each of the four cases. The slight differences between these values and those reported in Ref. 2 are due to (a) use of a more refined calculation of the scale factor used to convert the iron and carbon cross sections to free-proton cross sections, and (b) a better estimate of the attenuation length for π^- mesons in carbon. Quoted errors on the branching ratios are statistical. Although the four values are not statistically independent, correlations between them are expected to have a negligible effect on the branching ratio. Assuming no correlations, the best value for our branching ratio is the weighted mean of the four entries in Table II:

$$R = \Gamma(\rho^0 \to \mu^+\mu^-)/\Gamma(\rho^0 \to \pi^+\pi^-) = (5.6 \pm 1.1) \times 10^{-5}.$$

If the second and third determinations are assumed to be completely correlated then the uncertainty in the mean value is increased to $\pm 1.5 \times 10^{-5}$.

[15] J. D. Jackson and J. T. Donahue (private communication).

TABLE II. Four determinations of the branching ratio $\rho^0 \to \mu^+\mu^-/\rho^0 \to \pi^+\pi^-$.

Type of event	Muon-pair cross section ($\text{nb}=10^{-33}$ cm^2)	Restrictions	ρ^0-production cross section Source	Value (in $\mu\text{b}=10^{-30}$ cm^2)	$10^5\times$(branching ratio) [a]
2 prong from Fe, scaled to free proton	10.6±3.2	2 prong, $\lvert t\rvert<0.3$ (GeV/c)^2	hydrogen[b] bubble chamber	150±30	6.5±1.9
2 prong from C, scaled to free proton	9.4±3.2	2 prong, $\lvert t\rvert<0.3$ (GeV/c)^2	hydrogen[b] bubble chamber	150±30	5.7±1.9
2 prong from C, per C nucleus	6.0±1.7	2 prong, $\lvert t\rvert<0.3$ (GeV/c)^2	heavy-liquid[c] bubble chamber	121±68	4.6±2.9
all prong from C, per C nucleus	43.0±9.0	none	heavy-liquid[c] bubble chamber	716±200	5.3±1.9

[a] Best value for branching ratio $=(5.6\pm1.1)\times10^{-5}$ from combining all four values (see text).
[b] Reference 8.
[c] Reference 9.

Table III summarizes all ρ^0 leptonic branching ratios that have been reported in the literature. With regard to the colliding beams measurements, it is to be noted that the cross section for $e^+ + e^- \to \pi^+ + \pi^-$ at the peak of the ρ^0 resonance is related to the $\rho^0 \to e^+e^-$ branching by[16]

$$R=\Gamma(\rho^0 \to e^+e^-)/\Gamma(\rho^0 \to \pi^+\pi^-)=\sigma(e^+e^- \to \pi^+\pi^-)/3\pi\lambda\!\!\!^{-2}$$

with $\lambda\!\!\!^{-}$ the reduced wavelength of the colliding e^- (or e^+).

In principle a comparison of the branching ratios into muon and electron pairs provides a test of muon-electron universality. However, since the presently attainable precision is considerably less than required for such a comparison to be meaningful, branching ratios for both decay modes are listed together in the table. A summary of several of these measurements has been given by Ting.[17] All of the results save that of Hyams *et al.*[18] are in fair agreement within their quoted error limits. It is to be noted that the values of the spin-density matrix element ρ_{00} reported in Ref. 18 is in complete *disagreement* with the value obtained in the present experiment (Table I and Fig. 6). The two branching ratios determined from the electron-positron colliding beams experiments[19,20] are in principle the most reliable since these measurements are free of any strong-interaction effects.

The interest in these results follows from the suggestion that the ρ^0 meson dominates the π-meson form factor $F_\pi(q^2)$, and perhaps the isovector nucleon form factor as well. That such a dominance occurs at the ρ^0 resonance is obvious; the question arises: Does the ρ^0 meson dominate the π-meson form factor at $q=0$, where it is simply the π-meson charge and is precisely known? If so, the branching ratio can be quickly calculated. In the usual approximation that the width of the ρ^0 meson is small compared with the mass[21]:

$$R=\frac{\alpha^2}{36}\left(1-\frac{4M_\pi{}^2}{M_\rho{}^2}\right)^{3/2}\left(\frac{M_\rho}{\Gamma_\rho}\right)^2.$$

For the colliding beam experiments, where $F_\pi(q^2)$ is directly measured, a correction for finite width is easily

TABLE III. Summary of data on $\rho^0 \to l^+ + l^-$.

Group	Experiment	$10^5\times$(branching ratio)
This experiment	π^-+(Fe or C) $\to\mu^+ + \mu^-$	5.6±1.1
R. A. Zdanis *et al.*[a] (AGS)	$\pi^- + \text{H} \to e^+ + e^-$	$5.0_{-3}{}^{+6}$
J. K. dePagter *et al.*[b] (CEA)	$\gamma + \text{C} \to \mu^+ + \mu^-$	5.9±1.5[c]
M. Khachaturyan *et al.*[d] (Dubna)	$\pi^- + p \to e^+ + e^-$	3.9±1.2
B. Hymas *et al.*[e] (CERN)	$\pi^- + \text{H} \to \mu^+ + \mu^-$	$9.7_{-2.3}{}^{+2.0}$
J. Asbury *et al.*[f] (DESY)	$\gamma + \text{C} \to e^+ + e^-$	6.5±1.3
V. L. Auslander *et al.*[g] (Novosibirsk)	$e^+ + e^- \to \pi^+ + \pi^-$ (colliding beams)	4.9±1.0
J. E. Augustin *et al.*[h] (Orsay)	$e^+ + e^- \to \pi^+ + \pi^-$ (colliding beams)	6.2±1.0

[a] R. A. Zdanis, L. Madansky, R. W. Kraemer, S. Hertzbach, and R. Strand, Phys. Rev. Letters **14**, 721 (1965).
[b] Reference 13; J. K. de Pagter, J. I. Friedman, G. Glass, R. C. Chase, M. Gettner, E. von Goeler, R. Weinstein, and A. M. Boyarski, Phys. Rev. Letters **16**, 35 (1966). The branching ratio of these authors, given in this table, is somewhat different than the one quoted in this reference, and is taken from the summary data of Ref. 17.
[c] Assumes no ρ^0-ω^0 interference. See Ref. 13.
[d] M. N. Khachaturyan, M. A. Azimov, A. M. Baldin, A. S. Belousov, I. V. Chuvilo, R. Firkowski, J. Hladky, M. S. Khvastunov, J. Manca, A. T. Matyushin, V. T. Matyushin, G. A. Ososkov, L. N. Shtarkov, and L. I. Zhuravleva, Phys. Letters **24B**, 349 (1967).
[e] Reference 18.
[f] J. G. Asbury, U. Becker, W. K. Bertram, P. Joos, M. Rohde, A. J. S Smith, C. L. Jordan, and S. Ting, Phys. Rev. Letters **19**, 869 (1967).
[g] Reference 19.
[h] Reference 20.

[16] R. Gatto, in *Proceedings of the International Symposium on Electron and Photon Interactions at High Energies, Hamburg, 1965* (Springer-Verlag, Berlin, 1965), Vol. I, p. 106.
[17] S. Ting, in *Proceedings of the 1967 International Symposium on Electron and Photon Interactions at High Energies* (Stanford Linear Accelerator Center, Stanford, Calif., 1967), p. 452.
[18] G. Lütjens, U. Stierlin, and P. Weilhammer, Phys. Letters **24B**, 634 (1967).
[19] V. L. Auslander, G. I. Budker, Ju. N. Pestov, V. A. Sidorov, A. N. Skrinsky, and A. G. Khabakhpashev, Phys. Letters **25B**, 433 (1967).
[20] J. E. Augustin, J. C. Bizot, J. Buon, J. Haissinki, D. Lalanne, P. C. Marin, J. Perez-y-Jorba, F. Rumpf, E. Silva, and S. Tavernier, Phys. Rev. Letters **20**, 126 (1968).
[21] Y. Nambu and J. J. Sakurai, Phys. Rev. Letters **8**, 79 (1962); **8**, 191(E) (1962); M. Gell-Mann, D. Sharp, and W. Wagner, *ibid.* **8**, 261 (1962).

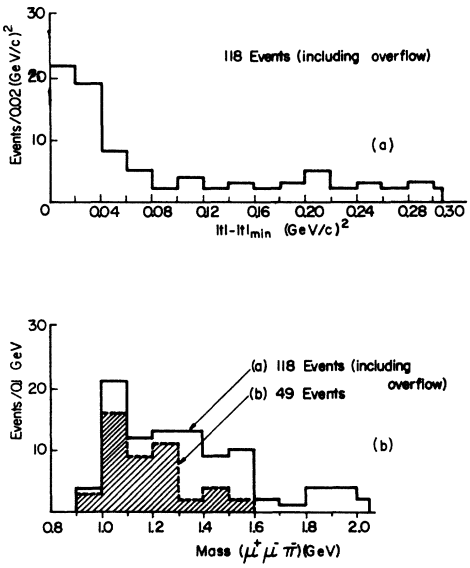

FIG. 7. (a) Momentum-transfer distribution for 118 three-pronged events on carbon subject to the restriction $600 \leq M_{\mu\mu} \leq 900$ MeV. (b) Invariant-mass spectrum for the $(2\mu)\pi^-$ system for three-pronged events on carbon with $600 \leq M_{\mu\mu} \leq 900$ MeV. Histogram (a) includes all 118 three-pronged events in that mass interval, histogram (b) includes only those with $|t| - |t|_{\min} < 0.06$ $(\mathrm{GeV}/c)^2$.

obtained. $F_\pi(q^2)$ must be analytic and obey a dispersion relation. A variety of forms satisfy this requirement. Gounaris and Sakurai[22] have given a detailed justification for one of these. However, it should be stressed that the argument for the correction is simpler and more general than used by these authors and depends solely on the existence of a smooth curve obeying a dispersion relation. Strictly speaking, these corrections only apply to measurements of $F_\pi(q^2)$ which is what the colliding beams measure. There may be further corrections of the same order for the other branching-ratio measurements.

The above-quoted vector-dominance relation involves two quantities that are not very precisely known, namely, the ρ^0 width and its leptonic branching ratio. The branching ratio and (93±15)-MeV width reported by the Novosibirsk colliding beams group[19] are in disagreement with the zero-width vector-dominance relation, while the larger branching ratio and (125±13)-MeV width from the Orsay experiment[20] are more nearly compatible with it. It is interesting to note that the (95±19)-MeV width reported in the present experiment is in good agreement with the Novosibirsk measurement, and certainly much smaller than the approximately 145-MeV width found in strong-interaction measurements.[23]

D. Three-Prong Events in Carbon

The apparatus used in the experiment was designed to accept ρ^0 mesons produced in the reaction $\pi^- + p \rightarrow \rho^0 + n$ with good efficiency, whereas reactions in which the ρ^0 was produced in association with an additional π^- meson were not emphasized. Nevertheless, an attempt was made to study the three-particle final state $\mu^+\mu^-\pi^-$ produced by incident π^- mesons on carbon. To this end, three-prong events were selected by requiring that no additional spark be present near the interaction vertex, a condition excluding both visible recoiling proton and nuclear break-up reactions. The precision of this selection criterion was limited by the thickness of spark-chamber plates. In addition, the two penetrating tracks were required to be tightly correlated with the tracks appearing in the range chamber (Sec. III).

Since there was no way to determine the charge of the outgoing particles, it was assumed that the two penetrating ones were muons of opposite sign and the third a π^- meson. The energies of the muons were determined by range, and of the π^- determined by assuming conservation of energy in the production of the three-particle final states. The latter hypothesis is well verified in coherent production experiments studying the production of $2\pi^-\pi^+$ when the four-momentum transfer is small.[24]

One-hundred fifty-five events satisfying the above scanning criteria were selected. Of these, 118 had an invariant dimuon mass in the ρ^0 range, i.e., $600 \leq M_{\mu\mu} \leq 900$ MeV. By imposing the further restriction $|t| - |t|_{\min} < 0.06$ $(\mathrm{GeV}/c)^2$ from the incident particle to the $\rho^0\pi^-$ system the number of events was reduced to 49. Figure 7(a) shows the 4-momentum transfer distribution for events with dimuon mass in the range $600 \leq M_{\mu\mu} \leq 900$ MeV. Figure 7(b) shows the $(2\mu)\pi^-$ invariant mass for dimuons in the same mass range with and without 4-momentum-transfer cuts imposed.

Some of the features already reported by bubble-chamber experiments are apparent in Figs. 7, namely, the rapidly falling 4-momentum-transfer dependence and the peaking of the three-particle invariant mass in the region immediately above 1 GeV.[24,25] However, the experimental resolution is insufficient for the extraction of information on the slope of the momentum-transfer dependence, nor is it possible to state with certainty that the three-particle invariant-mass histogram for small values of $|t| - |t|_{\min}$ does not contain some contamination from higher-momentum-transfer events.

The efficiency for detecting three-particle final states was of the order of a few percent for runs with the carbon-plate production chamber. Since the incident beam energy was lower during the iron runs while the thickness of absorber was approximately the same, acceptable three-prong events obtained in iron were less numerous than in carbon and suffered from more pronounced biases. In addition, the apparatus favored

[22] G. J. Gounaris and J. J. Sakurai, Phys. Rev. Letters **21**, 244 (1968).

[23] See, e.g., M. Roos, Nucl. Phys. **B2**, 615 (1967).

[24] J. F. Allard *et al.*, Phys. Letters **12**, 143 (1964); **19**, 431 (1965); Nuovo Cimento **46A**, 737 (1965).

[25] G. Goldhaber, in *Proceedings of the Thirteenth Annual International Conference on High-Energy Physics, Berkeley, 1966* (University of California Press, Berkeley, 1967), Session 7.

states in which the muons had equal energies and the π meson had a lower energy than either muon. Therefore, all the angular distributions are strongly biased and any attempt to apply fitting procedures as in the two-prong analysis (Sec. III) leads to very large errors both in the calculated angular distributions and in the cross section. Alternatively, when applying momentum cuts appropriate to these conditions to the heavy-liquid bubble-chamber events[9] (Sec. IV), the uncertainty in the minimum energy required introduces large errors in the number of surviving events. For this reason, it is difficult to estimate a $\rho^0 \rightarrow 2\mu$ branching ratio from this class of events alone, although the bubble-chamber data are relatively abundant. As already noted, however (Sec. V A), a Breit-Wigner resonance curve fit to the dimuon mass spectrum of these 155 three-pronged events yields an intrinsic width for the ρ^0 of 100 ± 23 MeV, in agreement with the intrinsic width determined from the two-prong events on iron.

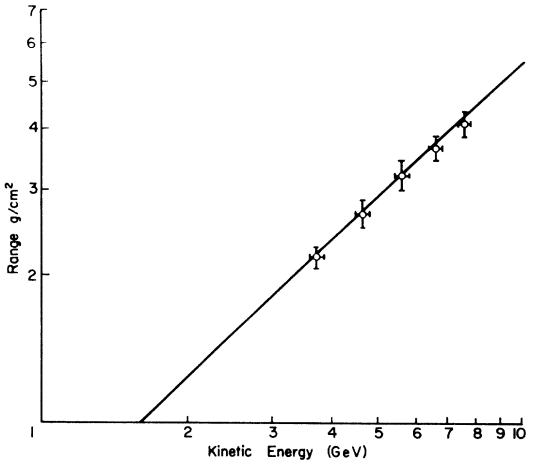

FIG. 8. Range of muons in iron. The experimental points were obtained by measuring the stopping positions of beam muons in the range-chamber array; the solid curve is based upon the work of Sternheimer (Refs. 30 and 32).

E. Additional Results

1. Possible Observation of Decay $\omega^0 \rightarrow \mu^+\mu^-$

Both the decay angular distributions for muon pairs in the dimuon rest system for $|t|>0.3$ (GeV/c)^2 (Ref. 2, Fig. 2) and the value of the density matrix element ρ_{00} for large momentum transfers are consistent with the production of the dimuon system by a vector-exchange mechanism.[12] This suggests that at least some of the muon-pair events for $|t|>0.3$ (GeV/)^2 are due to ω^0 decay. If this interpretation is correct, the dimuon mass spectra for these high-momentum-transfer events should be somewhat narrower than for those with lower momentum transfer. This feature is not exhibited by the data. Therefore, although the existence of the decay $\omega^0 \rightarrow 2\mu$ is certainly consistent with the angular distributions, there is no obvious way to obtain a clean sample of such events from these data and thus to determine a branching ratio.

2. Branching Ratio $\phi^0 \rightarrow 2\mu$

Reference 2 reported a peak containing 12 events in the dimuon mass spectrum produced by K^- mesons on both iron and carbon which was attributed to the decay mode $\phi^0 \rightarrow \mu^+\mu^-$. In Ref. 3, the total cross section for the production of ϕ^0 mesons incident on liquid hydrogen at 5.5 GeV/c was scaled as $1/p^2$ to 12 GeV/c. After making several appropriate corrections outlined in that reference, we reported

$$\Gamma(\phi^0 \rightarrow \mu^+\mu^-)/\Gamma(\phi \rightarrow \text{all}) = (3.5\times10^{-4})\times2^{\pm1}.$$

Several other measurements of this branching ratio have since appeared in the literature. A Dubna group[26] reports $(6.6_{-2.8}{}^{+4.4})\times10^{-4}$, a Rutherford Laboratory group[27] $(7.2\pm3.9)\times10^{-4}$, and a CERN group[28] $(4.5\pm1.7)\times10^{-4}$. These results are in fair agreement with $SU(3)$ expectations,[11,17] although their accuracy and the accuracy with which the ϕ^0 width is known are insufficient for a quantitative estimate.

3. Upper Limits on Two Rare Muon-Pair Decay Modes of the η^0 Meson

In Ref. 3, the dimuon mass spectrum for two-pronged events on iron was used to set upper limits on the branching ratios for two decay modes of the η^0 meson:

$$\Gamma(\eta^0 \rightarrow \mu^+\mu^-)/\Gamma(\eta^0 \rightarrow \text{all}) < 2\times10^{-5}$$

and

$$\Gamma(\eta^0 \rightarrow \pi^0\mu^+\mu^-)/\Gamma(\eta^0 \rightarrow \text{all}) < 5\times10^{-4}.$$

Both these upper limits are established at the 95% confidence level.

4. Absence of High-Mass $J=1^-$ Isovector Meson

Attempts to fit the isovector nucleon form-factor data using a resonance model had led to the suggestion that in addition to the ρ^0 meson there may exist a second $J=1^-$ isovector meson (the $\rho^{0\prime}$)with a mass in the neighborhood of 1 GeV.[29] The apparatus used in the present experiment had a reasonable efficiency for detecting dimuon states with invariant masses up to about

[26] R. G. Astvacaturov, M. A. Azimov, I. V. Chuvilo, J. Hladky, V. I. Ivanov, M. N. Khachaturyan, M. S. Khvastunov, A. T. Matyushin, V. T. Matyushin, L. I. Zhuravleva, A. M. Baldin, A. S. Belousov, and L. N. Shtrakov, Phys. Letters **27B**, 45 (1968).

[27] D. M. Binnie, A. Duana, A. R. Faruqui, J. P. Horsey, W. G. Jones, M. E. Kay, D. C. Mason, P. J. Nicholson, I. U. Rahman, J. Walters, J. G. Wilson, and P. Palit, Phys. Letters **27B**, 106 (1968).

[28] D. Bollini, A. Buhler-Broglin, P. Dalpiaz, T. Massam, F. Navach, F. L. Navarria, M. A. Schneegans, and A. Zichichi, Nuovo Cimento (to be published).

[29] For example, L. H. Chan, K. W. Chen, J. R. Dunning, Jr., N. F. Ramsey, J. Walker, and Richard Wilson, Phys. Rev. **141**, 1298 (1966).

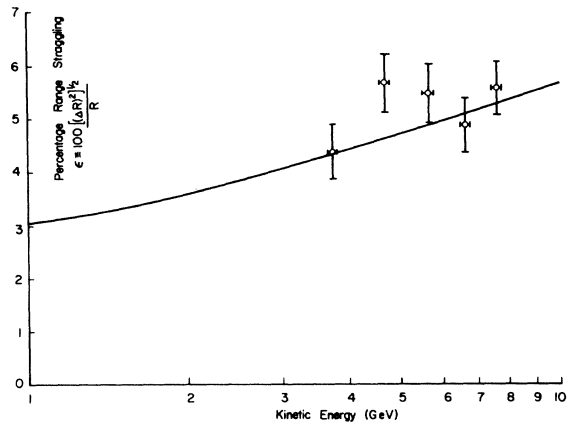

FIG. 9. Percentage range straggling of muons in iron. The solid curve is based upon the work of Sternheimer (Ref. 32).

1300 MeV. Therefore, the absence of any noticeable high-mass peak in the mass spectra (Figs. 4 and 5) implies that if such a meson exists its production cross section by 12-GeV/c π^- mesons is at least an order of magnitude smaller than the comparable ρ^0-production cross section.

Any vector meson which contributes to the π-meson form factor should be produced by one-pion exchange, as is the ρ^0 meson. Indeed, if the absorption corrections[12] could be reliably calculated, the present experiment could have been a direct measure of the π-meson form factor. It is hard to conceive that the absorption corrections could be far different for the $\rho^{0\prime}$ meson than for the ρ^0 meson. Thus this experiment shows that a $\rho^{0\prime}$ meson contributing significantly to the π-meson form factor must have a mass greater than about 1300 MeV. Unfortunately this mass threshold is too low to make a significant statement about the R meson, at 1620 MeV, which is postulated to be a ^3D state of two quarks and to have a spin and parity 1^-. Any new experiment should be designed to extend the range of this mass search in an attempt to shed light upon this tantalizing problem. A higher incident π-meson beam energy is the easiest way to insure this. Such an experiment would also have a better efficiency for detecting the $\pi^-\mu^+\mu^-$ states in the A_1 and A_2 mass regions.

ACKNOWLEDGMENTS

We acknowledge with gratitude the outstanding support given us by the staff of the Brookhaven National Laboratory, particularly by R. Cool and J. Sanford. T. Blair provided the liaison with the Alternating Gradient Synchrotron. R. Rubenstein and L. Read designed the 12-GeV/c negative beam and provided us with the required information about it. T. Kycia and R. Rubenstein made their Čerenkov counters available to us during the run. M. Schwartz loaned us most of the spark chambers from the Columbia-Brookhaven neutrino experiment for use as range chambers in our experiment.

APPENDIX: RANGE OF MUONS IN IRON

The range-chamber array used in this experiment was calibrated by setting the discriminator level on the slat counters so that one particle alone would trigger the system. Thus it was possible to photograph the stopping positions of the muons which constituted about 1–2% of the incident beam. Runs were taken at five different values of incident energy, and yielded an experimental range curve for muons with kinetic energies from 3.73 to 7.56 GeV. These data are in good agreement with the predictions of Sternheimer.[30–32]

The incident muon spectrum was assumed to consist of a narrow band corresponding to the muons which decayed upstream in the magnetic channel at a central momentum equal to the nominal momentum of the parent π meson, and a flat spectrum containing the muons from decays of π mesons after the last bending magnet immediately preceding the production chamber (Fig. 1). Thus the superposition of a Gaussian centered at the average momentum for muons within the narrow band superimposed upon a plateau consisting of the muons decaying after the last bending magnet was fitted to the experimental distributions. The central value of the Gaussian was assumed to represent the range, while its width was assumed to be the sum of the straggling error and the error derived from the finite thickness of the absorber plates.

The materials used as absorbers were rather heterogeneous, and included iron, lead, cast iron, aluminum, and alloyed steel. Furthermore, the density of some of them was known with limited precision. To obtain an equivalent stopping power for iron it was necessary to assume the ratios of stopping powers between different materials and iron at 4 GeV given in Refs. 30 and 31, to assume an average density for cast iron which neglected big bubbles in the samples used, and to assume a density for the alloyed steel suggested by its chemical composition (15% molybdenum).

The presence of a dead region (for reasons of construction) in all range chambers beyond the tenth module and the poor operation of the ninth chamber at the time of the calibrations set a bias toward lower ranges. An attempt was made to correct these biases by redistributing the excess events in the tenth chamber among the subsequent chambers, and by lumping together the events in the eighth and ninth chambers.

The calculated increase in path length due to multiple scattering and the effect of muon bremsstrahlung were found to be of negligible importance compared to errors from the above cited sources.

Figure 8 shows the experimental points on a plot of range versus kinetic energy. For comparison, a curve

[30] R. M. Sternheimer, Phys. Rev. **115**, 137 (1959).
[31] R. M. Sternheimer, Phys. Rev. **118**, 1045 (1960).
[32] R. M. Sternheimer, Phys. Rev. **117**, 485 (1960).

calculated by using the procedure of Ref. 30 and the ionization potential for iron of Ref. 32 is also given. The uncertainties in energy are estimated from the measured momentum width of the π-meson beam. Errors in range include straggling and the effects of the finite absorber thickness.

Figure 9 shows the experimental points on a plot of percentage straggling versus kinetic energy. For comparison, a curve based on a calculation of Refs. 32 and 33 for the percentage straggling in copper (which, in first approximation, should not be different from straggling in iron) is also given. The errors in energy are those noted above. Errors in percentage straggling arise from the finite absorber thickness and the limited statistical sample at each point.

[33] V. C. Burkig and K. R. MacKenzie, Phys. Rev. **106**, 848 (1957).

PHYSICAL REVIEW VOLUME 178, NUMBER 5 25 FEBRUARY 1969

η Production in the Reaction $\pi p \to \pi p \eta$ at 1050 and 1170 MeV/c†

RONALD A. GROSSMAN, LEROY R. PRICE, AND FRANK S. CRAWFORD, JR.
Lawrence Radiation Laboratory, University of California, Berkeley, California 94720

(Received 22 August 1968)

We have investigated η production in the reaction $\pi^+ p \to \pi^+ p \eta$ at 1050 and 1170 MeV/c, and in the reaction $\pi^- p \to \pi^- p \eta$ at 1170 MeV/c. We obtain the following partial cross sections for the reaction $\pi^\pm p \to \pi^\pm p \eta$ followed by the charged decay $\eta \to \pi^+ \pi^- \pi^0$: 9.5 ± 1.5 μb for 1050-MeV/c incident π^+; 53.3 ± 5.0 μb for 1170-MeV/c π^+; 15.9 ± 1.9 μb for 1170-MeV/c π^-. From our π^+ data we find that we need four $I = \frac{3}{2}$ amplitudes in order to obtain good agreement with our mass and angular distributions and to reproduce the threshold behavior of the cross section. We find the dominating amplitude to be that representing the reaction $\pi^+ p \to \eta \Delta(1238)$, $\Delta(1238) \to \pi^+ p$, where the η and the $\Delta(1238)$ are produced in s wave. The four amplitudes are extrapolated to higher energies where the predicted mass and angular distributions and cross sections are compared with the available data. From our π^- data we find that in addition to the four $I = \frac{3}{2}$ amplitudes (determined from the π^+ data), one $I = \frac{1}{2}$ amplitude is required: the amplitude in which all particles are in relative S states. We find that this $I = \frac{1}{2}$ amplitude in fact dominates the π^- reaction. We see no evidence for production of an $N^*(1550) \to \eta p$ resonance. We are able to parametrize the cross sections for $\pi p \to \pi p \eta$ from threshold to 4 BeV/c.

I. INTRODUCTION

SINCE the discovery of the η meson in 1961,[1] there have been several experiments[2–7] at various energies involving the reaction $\pi^+ p \to \pi^+ p \eta$. In all of these experiments the reaction appears to proceed mainly via

$$\pi p \to \eta \Delta(1238), \quad \Delta(1238) \to \pi p. \tag{1}$$

There have also been a few experiments[8–11] involving the reaction $\pi^- p \to \pi^- p \eta$.

Reaction (1) is unusual in that there are no pseudoscalar or vector mesons which can be exchanged in the t channel. Therefore, such models as the one-pion-exchange model or the vector-exchange model of

† Work done under the auspices of the U. S. Atomic Energy Commission.

[1] A. Pevsner, R. Kraemer, M. Nussbaum, C. Richardson, P. Schlein, R. Strand, T. Toohig, M. Block, A. Engler, R. Gessaroli, and C. Meltzer, Phys. Rev. Letters **7**, 421 (1961); also Pierre L. Bastien, J. Peter Berge, Orin I. Dahl, Massimiliano Ferro-Luzzi, Donald H. Miller, Joseph J. Murray, Arthur H. Rosenfeld, and Mason B. Watson, *ibid.* **8**, 114 (1962); D. Duane Carmony, Arthur H. Rosenfeld, and Remy T. Van de Walle, *ibid.* **8**, 117 (1962); Arthur H. Rosenfeld, D. Duane Carmony, and Remy T. Van de Walle, *ibid.* **8**, 293 (1962); M. Chrétien, F. Bulos, H. R. Crouch, Jr., R. E. Lanou, Jr., J. T. Massimo, A. M. Shapiro, J. A. Averell, C. A. Bordner, Jr., A. E. Branner, D. R. Firth, M. E. Law, E. E. Ronat, K. Strauch, J. C. Street, J. J. Szymanski, A. Weinberg, B. Nelson, I. A. Pless, L. Rosenson, G. A. Salandin, R. K. Yamamoto, L. Guerriero, and F. Waldner, *ibid.* **9**, 127 (1962).

[2] Horst W. J. Foelsche and Henry L. Kraybill, Phys. Rev. **134**, B1138 (1964).

[3] P. Daronian, A. Daudin, M. A. Jabiol, C. Lewin, C. Kochowski, B. Ghidini, S. Mongelli, and V. Picciarelli, Nuovo Cimento **41**, 502 (1966).

[4] Frederick E. James and Henry L. Kraybill, Phys. Rev. **142**, 896 (1966).

[5] C. Alff, D. Berley, D. Colley, N. Gelfand, U. Nauenberg, D. Miller, J. Schultz, J. Steinberger, T. H. Tan, H. Brugger, P. Kramer, and R. Plano, Phys. Rev. Letters **9**, 322 (1962); **9**, 325 (1962); C. Alff-Steinberger, D. Berley, D. Colley, N. Gelfand, D. Miller, U. Nauenberg, J. Schultz, T. H. Tan, H. Brugger, P. Kramer, and R. Plano, Phys. Rev. **145**, 1072 (1966).

[6] Maris Abolins, Richard L. Lander, Werner A. W. Melhop, Nguyen-huu Xuong, and Philip M. Yager, Phys. Rev. Letters **11**, 381 (1963).

[7] Benjamin Ching-Chun Shen, Lawrence Radiation Laboratory Report No. UCRL-16170, 1965 (unpublished).

[8] D. D. Carmony, F. Grard, R. T. Van de Walle, and Nguyen-huu Xuong, in *Proceedings of the International Conference on High-Energy Physics, 1962*, edited by J. Prentki (CERN Scientific Information Service, Geneva, 1962), p. 44.

[9] P. H. Satterbloom, W. D. Walker, and A. R. Irwin, Phys. Rev. **134**, B207 (1964).

[10] Suh Urk Chung, Orin I. Dahl, Janos Kirz, and Donald H. Miller, Phys. Rev. **165**, 1491 (1968).

[11] G. Ascoli, H. B. Crawley, D. W. Mortara, A. Shapiro, C. A. Bridges, B. I. Eisenstein, U. E. Kruse, E. D. Schafer, and B. Terreault, Phys. Rev. Letters **20**, 1321 (1968).